NONLINEAR OPTICS AT UMER: LESSONS LEARNED IN SIMULATION

K. Ruisard[*], Oak Ridge National Laboratory, Oak Ridge, Tennessee
B. Beaudoin, I. Haber, D. Matthew, and T. Koeth,
Institute for Research in Electronics and Applied Physics, College Park, Maryland

Abstract

Design of accelerator lattices with nonlinear optics to suppress transverse resonances is a novel approach and may be crucial for enabling low-loss high-intensity beam transport. Large amplitude-dependent tune spreads, driven by nonlinear field inserts, damp resonant response to driving terms. This presentation will focus on simulations of the UMER lattice operated as a quasi-integrable system (one invariant of transverse motion) with a single strong octupole insert. We will discuss the evolution of simulation models, including the observation of losses associated with the original operating point near a fourth-order resonance. Other operating points farther from this resonance are considered and shown to be more promising.

INTRODUCTION

Nonlinear integrable optics (NLIO) is a novel implementation of focusing optics for accelerator rings. Proposed by Danilov and Nagaitsev [1], this technique is expected to mitigate resonant beam losses in circular machines. This is of particular interest at the "intensity frontier," where even low-level losses can threaten machine components and personnel safety.

Nonlinear terms in the transverse focusing potential have long been known to counteract resonant interactions in rings. In the presence of nonlinear forces, the coupling of regular driving terms to particle orbits is reduced and collective motions such as envelope modes decohere. The most well-known example is octupole-induced Landau damping, in which an octupole-induced tune shift in the particle distribution can damp transverse collective instability [2]. Simulation studies of NLIO systems shows fast decoherence of envelope modes, which are a known mechanism for halo formation [3].

In general, introducing nonlinearities reduces dynamic aperture due to chaotic orbits near resonance overlap, which has previously restricted the use of nonlinear correctors to weak perturbations of the linear Hamiltonian. The breakthrough of NLIO is the identification of a family of highly nonlinear, physically-realizable magnetic potentials in which transverse particle orbits conserve coupled, quadratic invariants of motion that are distinct from the Courant-Snyder invariants.

This paper describes progress towards an experimental demonstration of quasi-integrable optics (QIO) at the University of Maryland Electron Ring (UMER). This variation on the NLIO theory utilizes an octupole potential (rather than the fully-integrable fields discussed in reference [1]) that allows one invariant of transverse motion: the Hamiltonian in normalized coordinates[1]:

$$H_N = \frac{1}{2}\left(p_{x,N}^2 + p_{y,N}^2 + x_N^2 + y_N^2\right) + \frac{\kappa}{4}\left(x_N^4 + y_N^4 - 6y_N^2 x_N^2\right). \quad (1)$$

Although motion is not fully integrable (only one invariant for 2D motion), the invariant corresponds with particle amplitude resulting in chaotic but bounded motion [3].

This proceedings discusses simulation results for the QIO as designed for UMER. We probe dynamics within the octupole insert "as designed" and show clear improvement for one insert configuration over another. We also compare transport properties across a range of tune operating points while seeking to maximize octupole-induced tune spread and preserve stable particle orbits.

NONLINEAR OPTICS PROGRAM AT UMER

UMER is a scaled, 10 keV ($\beta = 0.195$) electron ring designed for the study of high-intensity beam dynamics relevant to higher-energy ion rings. Different space charge densities are selected by aperturing the beam near the source, in the range $\nu/\nu_0 = 0.85 \rightarrow 0.14$ for nominal UMER tune 6.7 (incoherent shifts $\Delta\nu = 0.3 \rightarrow 5.7$) [4, 5].

A proof-of-principle QIO experiment has been designed for UMER. The experiment layout, shown in Figure 1, includse a single octupole insert element. This effort uses existing UMER quadrupole optics to meet requirements for linear lattice focusing, which are outlined below. The RMS envelope solution for the linear optics as designed is shown in Figure 2. Details of implementing this solution in the UMER ring are discussed in references [6, 7]. A custom-designed octupole insertion, consisting of seven independently-wired octupole PCBs, has been fabricated and is capable of meeting requirement 2 to within RMS error of 2%. Design of the octupole element is covered in reference [8].

For initial tests of the QIO concept, we desire beams with lower space-charge tune shift than the typical UMER range, as the NLIO/QIO theory is based on single-particle dynamics. An ultra-low-current, high emittance beam was characterized for use in initial experiments. A beam with current 10 to 100 µA is generated by operating the UMER triode electron gun in voltage amplification mode. This beam has low tune shift due to its large emittance; quadrupole scan emittance measurement at 40 µA output current returns

---

[*] ruisardkj@ornl.gov

[1] $x_N \equiv \frac{x}{\sqrt{\beta_x(s)}}, p_{x,N} \equiv p_x \sqrt{\beta_x(s)} + \frac{\alpha_x x}{\sqrt{\beta_x(s)}}$
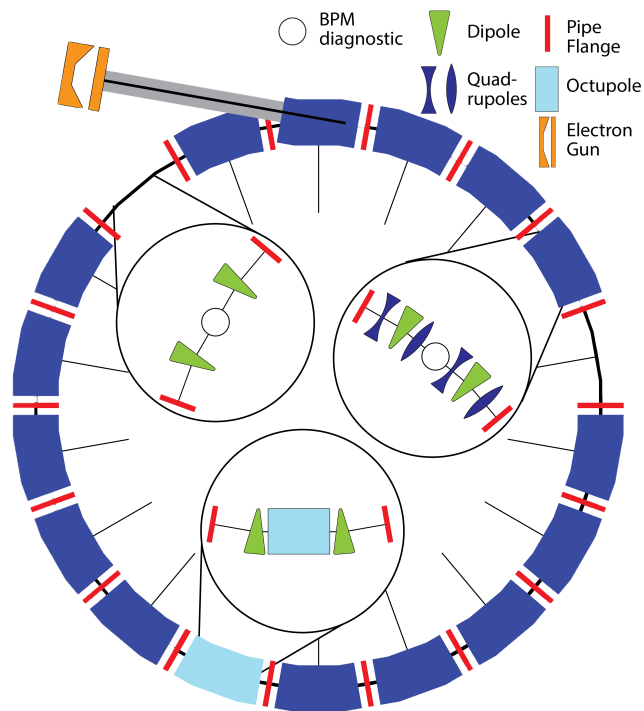
Figure 1: Diagram of UMER QIO lattice, with insets showing detail for standard 20° section (Q-D-Q-Q-D-Q) and octupole section (0-D-OCTU-D-0). Spokes indicate diagnostic locations and red bands indicate flange locations.

$\epsilon_x = 300$ mm-mrad, $\epsilon_y = 100$ mm-mrad (unnorm., 4×RMS). For the simulations discussed here, a $100\,\mu$m, $60\,\mu$A semi-Gaussian beam is used as the test case.

Choice of Operating Point

The building blocks of a NLIO/QIO lattice are nonlinear insertion elements embedded within a linear-focusing (quadrupole) lattice, which is required for transverse confinement. The conditions for integrability are:

1. Beam envelope is round through the nonlinear insertion ($\beta_x = \beta_y$); this is done by forming a round waist β_* in the nonlinear insert.

2. Nonlinear potential is scaled to cancel s-dependence of H_N (for QIO, $G_3(s) \propto \beta^{-3}(s)$); this is required for normalized orbits to move through a constant potential.

3. Linear-focusing transport between insertions must have phase advance $n\pi$; this is required for particle motion to be quasi-continuous in the nonlinear potential.

Choice of lattice operating tune is constrained mainly by the minimum achievable waist size, β_*, given the existing quadrupole optics. $\beta_* = 0.3$ was identified as a "safe" waist size, with 2× edge distance to the pipe wall at the largest transverse beam extent.

Original plans for nonlinear UMER included a "segmented" 64-cm octupole channel over a UMER 20° section,
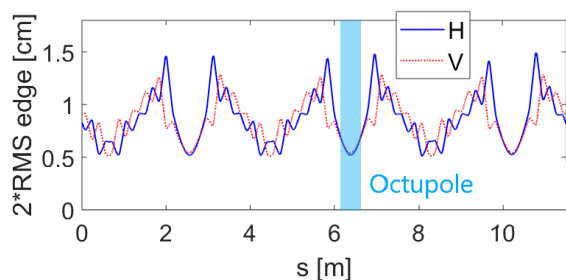
Figure 2: Periodic KV envelope solution for 100 mm-mrad, $60\,\mu$A beam at $\nu_x = \nu_y = 3.26$. Injection is at $s = 0$ plane.

which encompasses two 10° bends. This lattice would have fractional tune 0.263 to meet the quasi-integrable condition; this fractional tune also corresponds with the maximum theoretical tune spread. Restricting the channel length to 25 cm (the longest contiguous element that can be placed in UMER) reduces the maximum achievable tune spread from 0.26 to 0.13.

As seen in Figure 3, the largest accessible tune operating point that can be achieved for a large-emittance beam and 25-cm insert with existing optics is ~ 0.35. Higher tunes require either a smaller waist size β_*, which will lead to scraping, or use of multiple insert regions, which is not considered at this time but may be possible as an extension of this work.

Simulation Models

In order to isolate dynamics within the nonlinear potential, PIC simulations with the WARP code [9] are performed on a "simple model" of the QIO system. This simple model consists only of the octupole element and an ideal, thin lens, symmetric focusing kick as a proxy for the linear focusing sections. Effects accruing over the length of the lattice (such as the space charge force) are excluded in this model. We also examine PIC simulation over full QIO experiment configuration included linear optics modeled as hard-edged quadrupoles. In the ring model used here, dipoles are excluded for simplicity. The UMER dipoles introduce a significant linear focusing component due to fringe fields and a sextupole term in the PCB dipole circuits. For the insert, we alternately use an ideal octupole potential or a gridded field element representative of the octupole channel as de-
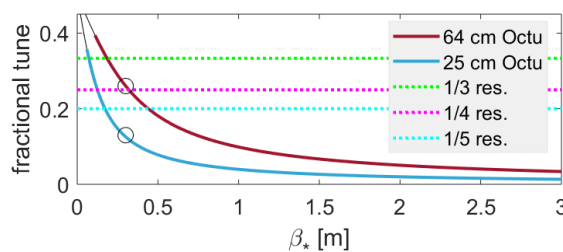
Figure 3: Accessible tune operating points as a function of β_* waist size in a single-channel UMER QIO lattice. Circles indicate nominal operating points at $\beta_* = 0.3$ m.
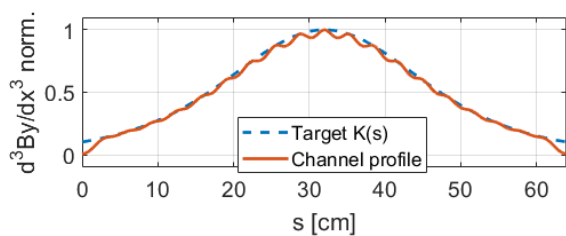
(a) Octupole channel assuming full population of 20° arc.
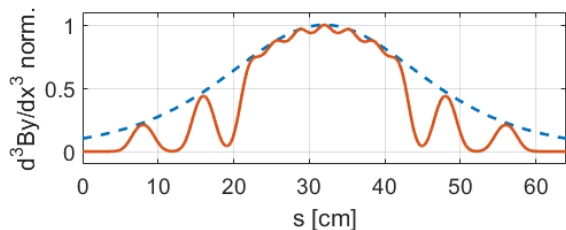
(b) Octupole channel with clearance for mounts, including octupole circuits co-housed with dipoles.
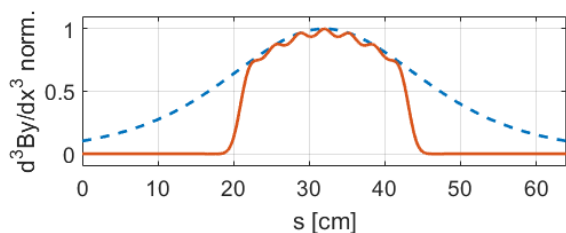
(c) Octupole channel restricted to straight section between dipoles.

Figure 4: Octupole channel profile configurations. While 4(a) is ideal, only 4(b) and 4(b) are realizable in the experiment.

signed, which is generated by the Biot-Savart solution for the PCB circuit. 40,000 macro-particles are used in the space-charge model, while the frequency map is sampled using a zero-charge, gridded "witness distribution."

CHOOSING OCTUPOLE INSERT CONFIGURATION

Adding an octupole insertion to UMER can be done by modifying a single, modular 20° (64 cm) arc. As mentioned, initial designs assume a fully-occupied but segmented arc, in which octupoles are placed at every available location with gaps for mechanical clearance. The desired octupole profile $d^3 B_y(s)/dx^3 \propto \beta^{-3}(s)$ (Requirement 2) is painted in along the "octupole section" using short (4.65 cm) PCB magnets. Three configurations are shown in Fig. 4. The scheme shown in Fig. 4(a) is purely hypothetical, as the presence of two bending dipoles in the arc restrict octupole PCB placement.

The three cases shown in Fig. 4 were compared using the dipole-free simple model with thin-lens focusing and gridded fields from Biot-Savart solution of the octupole circuits (the added complication of introducing bends is ignored in this analysis). The resulting frequency map for
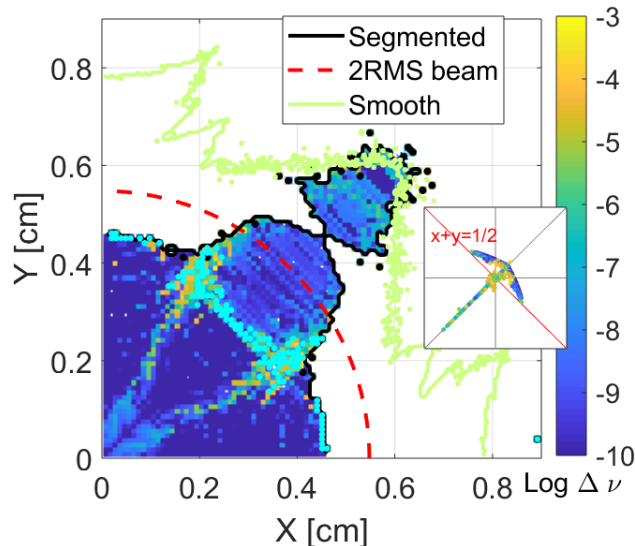
(a) Configuration space plot of aperture and resonant structure.
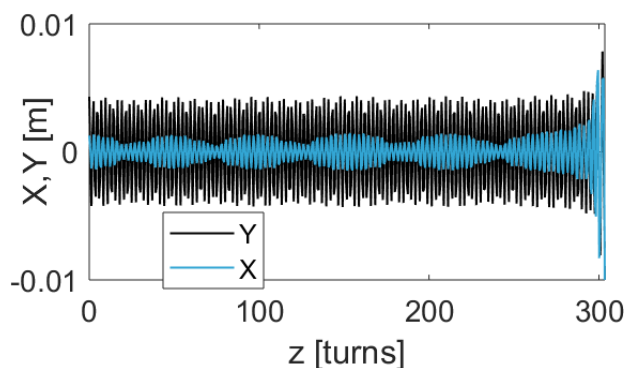
(b) X and Y trajectory of particle at edge of stable boundary. Particle initial condition is indicated on Fig. 5(a).

Figure 5: Frequency map of simple QIO lattice at peak field 50 T/m³ ($\kappa = 3984$) and fractional tune 0.26 for 1024 passes. Light green countour/footprint indicates the smooth, 64 cm channel (Fig. 4(a)).

1024 passes with peak field 50 T/m³ ($\kappa = 3984$) is shown in Fig. 5. Very poor performance is seen in the "segmented channel" (Fig. 4(b)) as compared to the other configurations shown, even before considering the effect of bends.

Particles appear to be lost along the $\nu_x + \nu_y = 1/2$ coupling resonance. Figure 5(b) shows a typical orbit of a particle near the stable boundary, where the small-amplitude plane quickly grows after some length of time. As a result of this poor performance seen here, plans for a 64-cm "segmented" octupole insertion are discarded, and the design shifts to a 25-cm, 10° insert.

BEAM STABILITY IN QIO UMER RING

Simulation of the proposed experiment over the full ring is done both at the original operating point based on the assumption of a 64 cm octupole insert (fractional tune 0.263) and at a new operating point adjusted for a shorter insert

(fractional tune 0.126). As stated above, dipole effects are ignored in these test cases and all elements are hard-edged. For the proposed experiments, a peak octupole gradient of 50 T/m^3 places the fixed point at 3.2σ (for a beam with of 100 mm-mrad 4×RMS emittance). This requires only 0.97 A in the central octupole circuit, well within the safety limit of the UMER octupoles.

PIC Simulation at Nominal 3.26 Operating Point

The first full ring simulations were run at the original operating point with fractional tune 0.26. Figure 6 shows results from a 60 μA beam at the initial design tune of $\nu_{0,x} = \nu_{0,y} = 3.26$. Large loss of stable aperture is seen when compared to the 64-cm simple model. This tune is also very near the fourth order $\nu = 0.25$ resonance, which is strongly driven by the octupole term. Although not an feature seen in simple model calculations, the beam distribution shown in Fig. 6(c) depicts clear fourth-order resonant structure. However, the boundary of stable orbits corresponds with the $\nu_y + \nu_x = 1/2$ coupling resonance rather than $\nu = 0.25$. The reduced stability may be due to overlap between these two conditions.

In the case shown here, the octupole insert length is limited to 25-cm to correspond with the channel as designed. This places the operating point quite far from the quasi-integrable condition $\psi = n\pi$. This is reflected in the large fluctuations in the quantity H_N (Eq. (1)), which on average over all stable orbits exhibits 8.02% variation.

PIC Simulation at $\nu = 0.13$

In comparison, adjusting the linear optics to shift the tune towards the quasi-integrable condition at $\nu_x = \nu_y = 3.13$ yields much better transport. The envelope solution is similar to that shown in Fig. 2 so the adjusted case is not reproduced here. As shown in Fig. 7, the dynamics agree well with simple model predictions. The enhanced stability is reflected in better conservation of H_N. A less than 1% variation is observed for all particles in the zero-charge limit. An average 4% variation is seen when the 60 μA current is included, but this is mainly due to contribution from low-amplitude, highly-depressed particles (see discussion in conclusion section). The main drawback is that operating at lower tune puts a limit on the maximum stable tune spread, which is reduced from ~0.26 to ~0.13.

A Comment on Space Charge

Simulations were run with the low-charge, high-emittance 60 μA beam, which has a predicted incoherent tune spread of 0.005. Compared to the "zero-charge" case, the effect of space charge on the stable aperture and induced tune spread is small. However, variation of the quantity H_N increased in the presence of space charge. Figure 8 shows the dependence of H_N variation on initial particle radius r (comparable to particle amplitude). While there is no trend in the "zero-charge" case, when the 60 μA current is considered variation increases, with the largest variations occuring at small amplitudes (the most shielded particles).
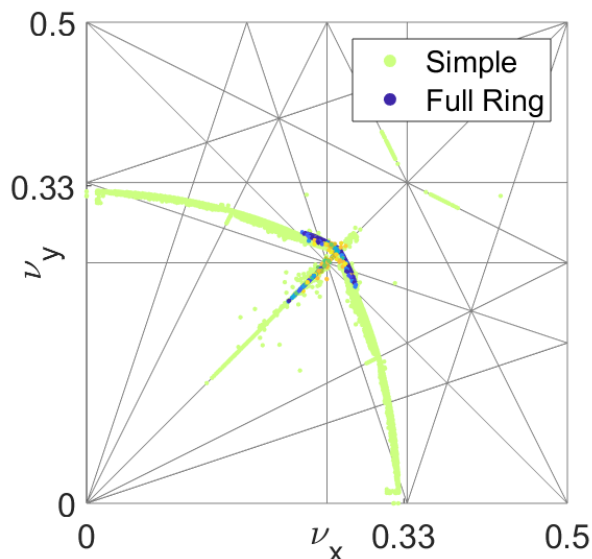
(a) Tune footprint with up to fourth order resonance lines indicated.
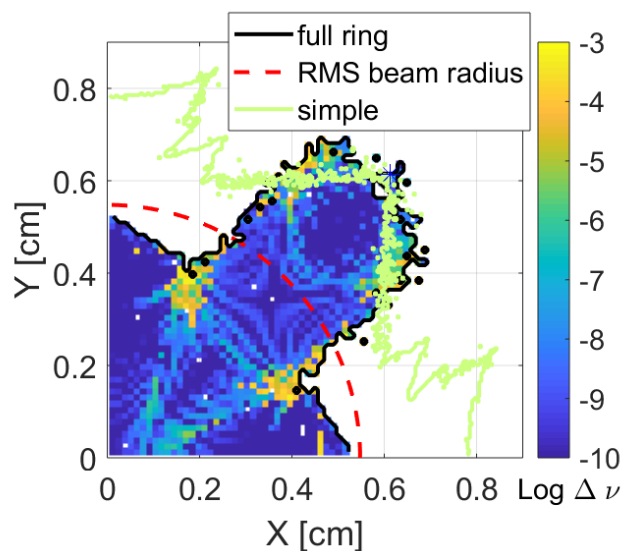
(b) Configuration space plot of aperture and resonant structure.
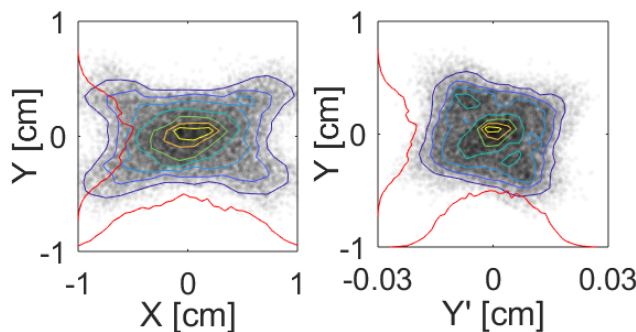
(c) Snapshot of beam distribution at turn 128 showing clear fourth-order resonance structure.

Figure 6: Frequency map of QIO lattice at peak field 50 T/m^3 ($\kappa = 2390$) and fractional tune 0.26 at turn 384. Best-case simple model is compared with hard-edged model of full ring.

(a) Tune footprint with up to fourth order resonance lines indicated.

(b) Configuration space plot of aperture and resonant structure.

(c) Snapshot of beam distribution at turn 264.

Figure 7: Frequency map of QIO lattice at peak field 50 T/m^3 ($\kappa = 3984$) and fractional tune 0.13 at turn 896.
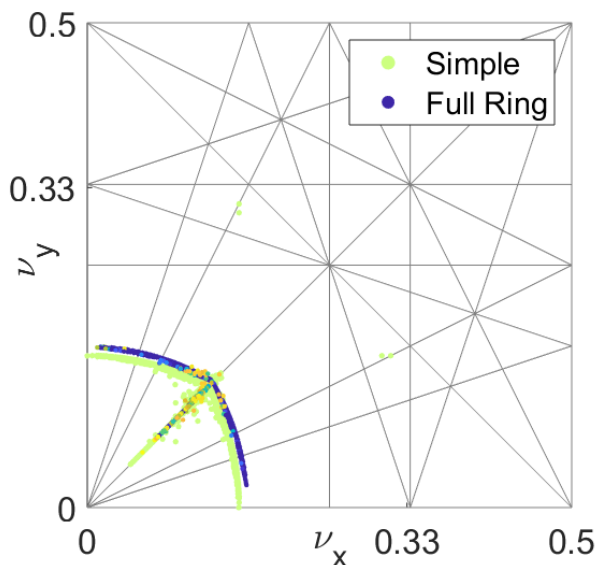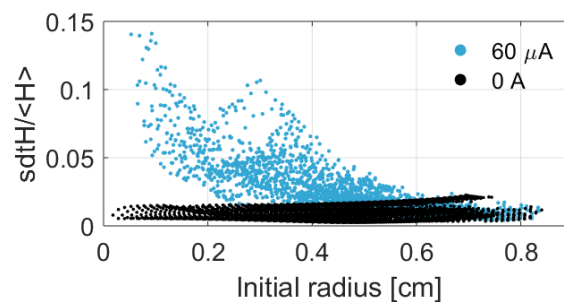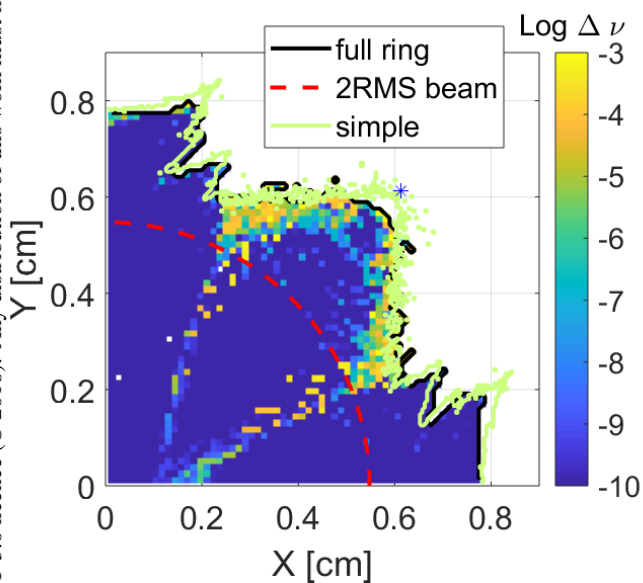
Figure 8: Dependence of H_N variation on initial orbit radius r after 264 turns in the $\nu = 3.13$ QIO lattice.
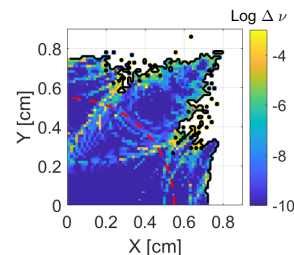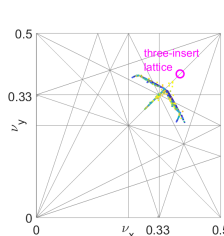
(a) Tune footprint with up to fourth order resonance lines indicated.

(b) Configuration space plot of aperture and resonant structure.

Figure 9: Frequency map of QIO lattice at peak field 50 T/m^3 ($\kappa = 3984$) and fractional tune 0.35 at turn 384. Asymmetry is due to tune error $\nu_x - \nu_y = 0.01$.

However, these orbits appear to remain bounded. For the work shown here, linear optics were optimized for quasi-integrable transport of an equivalent KV beam (in other words, optimized for the maximally depressed particle orbit).

Alternative Operating Points for Increased Tune Spread

Two strategies for increasing the octupole-induced tune spread are considered. In the first, the fractional tune is increased by adjusting the focusing of the linear optics. Second, fractional tune is increased by reducing waist size β_*. Results shown in this section are calculated in the zero-charge limit.

Figure 9 shows transport results for a lattice at tune $\nu = 3.35$, which is achieved by adjusting linear optics without changing envelope properties in the octupole section. Dynamics appear very similar to the case as $\nu = 3.13$, with a slight asymmetry due to unequal tunes in this solution ($\nu_x - \nu_y = 0.01$). The variation of H_N is larger in this case, 1.3%, but this is expected as the QI condition is not met. However, this design is near the tune $\nu = 3.39$ where installing three insertions (one at each waist) satisfies the QI condition. Multi-insert configurations may be considered to enhance the tune spread near this operating point in future work.

Tune for the single-channel lattice can also be increased by decreasing waist size β_*. This can be achieved for the 25-
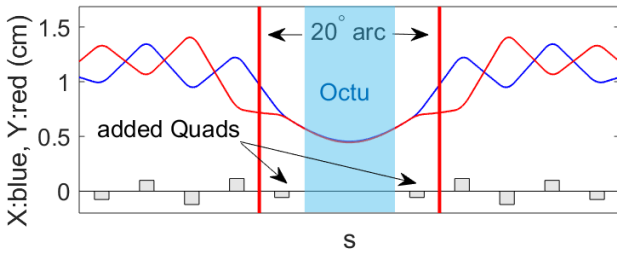
Figure 10: Alternative lattice solution included additional quads placed in same 20° section as octupole insert.
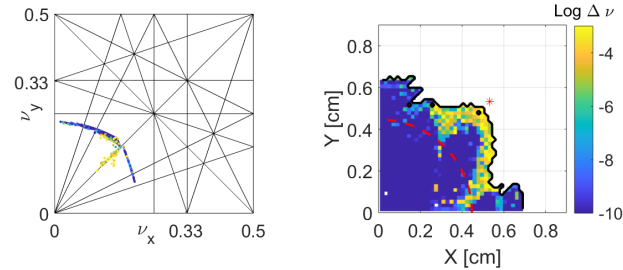
(a) Tune footprint with up to fourth order resonance lines indicated.

(b) Configuration space plot of aperture and resonant structure.

Figure 11: Frequency map of QIO lattice at peak field 150 T/m^3 ($\kappa = 3514$) and fractional tune 0.18 at turn 512.

cm insertion by placing quadrupoles nearer the insertion as shown in Fig. 10 (In the previous cases, these locations were unoccupied drifts). Figure 11 shows the case for $\beta_* = 0.2$ m, $\nu = 3.18$ and Fig. 12 shows $\beta_* = 0.16$ m, $\nu = 3.23$. In both cases the peak octupole field must be increased to 150 T/m^3 to maintain a large tune spread in the beam distribution. This requires 2.92 A in the octupole PCB, which is near the safety limit for UMER magnets. 6.4 A is required to achieve κ equal to the cases shown above, which is possible with water cooling to protect the magnet circuit.

SUMMARY AND CONCLUSION

In this investigation, multiple operating points are explored for use in the UMER QIO experiment. Results for
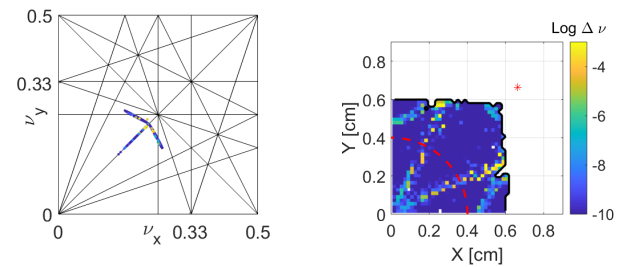
(a) Tune footprint with up to fourth order resonance lines indicated.

(b) Configuration space plot of aperture and resonant structure.

Figure 12: Frequency map of QIO lattice at peak field 150 T/m^3 ($\kappa = 1813$) and fractional tune 0.22 at turn 512.

all cases are summarized in Table 1. Shifting of operating points is motivated in part by a study of various octupole channel configurations. The original design included a "segmented" 64-cm octupole insert, in which a long, straight insert is flanked by single octupole magnets as space allows. This was found to be very detrimental to lattice stability, and plans were shifted to focus on a single, 25-cm straight insert.

In full ring simulations, the original operating point of $\nu = 3.26$ is found to have poor transport, due both to proximity to the driven fourth-orders resonance and violation of the QI condition. A more promising result is found at $\nu = 3.13$ for the single-insert configuration. However, the maximum possible tune spread is halved as a result. To remedy this, we explore the possibility of increasing the operating tune (and therefore the tune spread) by adjusting optics outside and inside the insertion region. Increasing tune advance through the octupole by decreasing waist size β_* is limited by safety limits on octupole circuit heat load. However, adjusting for a higher tune with three insertions is promising, and may warrant further investigation.

Table 1: Predicted performance of two tune operating points for PIC simulation of QIO ring with hard-edged elements and peak octupole gradient 50 T/m^3 ($\kappa = 3948$). Conservation of invariant $\langle H_N \rangle / H_N$ is taken as average over all stable particle orbits within the 2×RMS beam radius.

		max/RMS		
ν	β_* [m]	σ_ν	eff. r_{max}	$\left\langle \frac{\langle H_N \rangle}{H_N} \right\rangle$ [%]
0.26	0.30	0.017/0.006	0.48 cm	8.02
0.13	0.30	0.064/0.019	0.67 cm	0.92
0.35	0.30	0.062/0.019	0.65 cm	1.32
0.22 *†	0.16	0.056/0.019	0.58 cm	3.64
0.18 *‡	0.20	0.063/0.021	0.54 cm	14.47

∗ Peak field 150 T/m^3
† $\kappa = 1813$
‡ $\kappa = 3514$

ACKNOWLEDGMENTS

REFERENCES

[1] V. Danilov and S. Nagaitsev, "Nonlinear accelerator lattices with one and two analytic invariants," *PRSTAB*, vol. 13, no. 8, p. 084 002, Aug. 2010.

[2] A. W. Chao, *Physics of Collective Beam Instabilities in High Energy Accelerators*. John Wiley & Sons, 1993.

[3] S. D. Webb, D. L. Bruhwiler, A. Valishev, S. N. Nagaitsev, and V. V. Danilov, "Chromatic and Dispersive Effects in Nonlinear Integrable Optics," in *Proceedings of HB2014*, East-Lansing, MI, 2014, p. 10.

[4] R. A. Kishek *et al.*, "The University of Maryland Electron Ring Program," *Nuclear Instruments and Methods in Physics Research, Section A: Accelerators, Spectrometers, Detectors and Associated Equipment*, vol. 733, pp. 233–237, 2014.

[5] S. Bernal *et al.*, "Ultra-low current beams in UMER to model space-charge effects in high-energy proton and ion machines," in *AIP Conf. Proc.*, vol. 1812, National Harbor, MD: AIP, 2017, p. 110 006.

[6] K. J. Ruisard *et al.*, "Tuning low-current beams for nonlinear quasi-integrable optics experiments at the University of Maryland Electron Ring," in *Proceedings of IPAC2018*, 2018, pp. 3585–3588.

[7] K. Ruisard, H. Baumgartner, B. Beaudoin, I. Haber, M. Teperman, and T. Koeth, "Experimental plans for single-channel strong octupole fields at the University of Maryland Electron Ring," in *Proceedings of NAPAC2016*, paper TUPOB12, Chicago, IL, 2016, pp. 507–510.

[8] H. Baumgartner *et al.*, "Quantification of octupole magnets at the University of Maryland Electron Ring," in *Proceedings of NAPAC2016*, Chicago, IL, 2016, pp. 503–506.

[9] A. Friedman *et al.*, "Computational methods in the warp code framework for kinetic simulations of particle beams and plasmas," *IEEE Transactions on Plasma Science*, vol. 42, no. 5, pp. 1321–1334, 2014.

[10] H. Baumgartner, K. Ruisard, D. Matthew, T. Koeth, I. Haber, and B. Beaudoin, "Initial tests of nonlinear quasi-integrable optics at the university of maryland electron ring," in *Proceedings of IPAC18*, Vancouver, Canada, 2018.

[11] S. Antipov *et al.*, "IOTA (Integrable Optics Test Accelerator): facility and experimental beam physics program," *J Instr*, vol. 12, no. 03, Mar. 2017.